JACS
JOURNAL OF THE AMERICAN CHEMICAL SOCIETY

ARTICLE

pubs.acs.org/JACS

Temperature-Dependent Spin Crossover in Neuronal Nitric Oxide Synthase Bound with the Heme-Coordinating Thioether Inhibitors

Tzanko Doukov,[‖] Huiying Li,[‡] Ajay Sharma,[§] Jeffrey D. Martell,[§] S. Michael Soltis,[‖] Richard B. Silverman,[†] and Thomas L. Poulos*[,‡]

[‡]Departments of Molecular Biology and Biochemistry, Pharmaceutical Sciences, and Chemistry, University of California, Irvine, California 92697-3900, United States

[‖]Macromolecular Crystallographic Group, Stanford Synchrotron Radiation Lightsource, SLAC, Stanford University, Stanford, California 94309, United States

[†]Department of Chemistry, Department of Molecular Biosciences, Chemistry of Life Processes Institute, and Center for Molecular Innovation and Drug Discovery, Northwestern University, Evanston, Illinois 60208-3113, United States

[§]Department of Chemistry, Northwestern University, Evanston, Illinois 60208-3113, United States

ABSTRACT: A series of L-arginine analogue nitric oxide synthase inhibitors with a thioether tail have been shown to form an Fe−S thioether interaction as evidenced by continuous electron density between the Fe and S atoms. Even so, the Fe−S thioether interaction was found to be far less important for inhibitor binding than the hydrophobic interactions between the alkyl group in the thioether tail and surrounding protein (Martell et al. J. Am. Chem. Soc. 2010, 132, 798). However, among the few thioether inhibitors that showed Fe−S thioether interaction in crystal structures, variations in spin state (high-spin or low-spin) were observed dependent upon the heme iron oxidation state and temperature. Since modern synchrotron X-ray data collection is typically carried out at cryogenic temperatures, we reasoned that some of the discrepancies between cryo-crystal structures and room-temperature UV−visible spectroscopy could be the result of temperature-dependent spin-state changes. We, therefore, have characterized some of these neuronal nitric oxide synthase (nNOS)−thioether inhibitor complexes in both crystal and solution using EPR and UV−visible absorption spectrometry as a function of temperature and the heme iron redox state. We found that some thioether inhibitors switch from high to low spin at lower temperatures similar to the "spin crossover" phenomenon observed in many transition metal complexes.

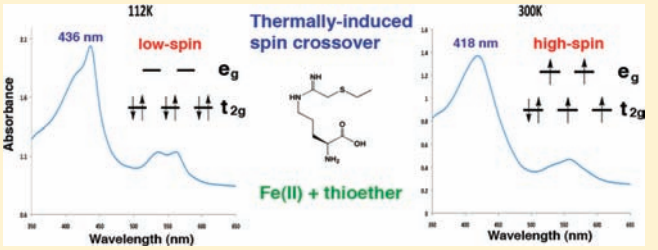

INTRODUCTION

Nitric oxide synthases (NOSs) are a family of cysteine-thiolate ligated heme and flavin containing enzymes in mammals that produce nitric oxide (NO) using L-arginine as a substrate in the presence of O_2 and NADPH.[1,2] NO generated from three different NOS isoforms, neuronal NOS, endothelial NOS, and inducible NOS, functions as either a vital signaling molecule in the neural and cardiovascular systems or a cytotoxic agent in the immune system, respectively. However, unregulated NO production has been associated with various pathological conditions.[3,4] Utilizing NOS inhibitors, especially those with high potency and isoform selectivity, to control unwanted NO generation under a pathological condition might be beneficial in the treatment of NO related diseases.[5,6]

In our ongoing efforts to develop isoform-selective NOS inhibitors, we have been interested in finding compounds that not only bind to the substrate binding pocket but also coordinate directly to the heme iron in order to improve potency. We reported earlier[7] a series of substrate analogue inhibitors each of which bears a potential N-donor or S-donor heme ligand.

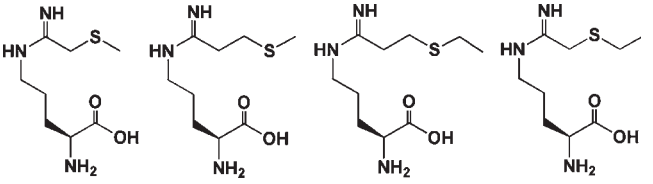

1 **2** **3** **4**

However, all of these compounds, including thioether compounds **1** and **2**, exhibited modest binding affinity and formed high-spin complexes, as measured by solution UV−visible spectroscopy at room temperature, indicating no iron coordination. On the basis of those results, we recently developed a new series of thioether compounds[8] and used UV−visible absorption spectrophotometry and crystallography to determine whether the thioether sulfur can directly coordinate to the heme iron.

Received: February 28, 2011
Published: May 02, 2011

The key observations from these studies were as follows: (a) Compounds **1** and **2** are type I (high-spin) inhibitors as determined by spectral shift assays[7] and, in the case of **1**, confirmed by crystal structures.[8] However, extending the tail group of the thioether from a methyl in **1** or **2** to an ethyl allowed the resulting compounds (**3** or **4**) to coordinate the heme iron and form low-spin complexes. The newly established hydrophobic contacts from the ethyl group to the protein stabilize Fe−S thioether coordination. (b) The coordination of thioether inhibitors to the heme iron did not increase inhibitory potency. (c) While compound **3** could coordinate to the heme iron regardless of the heme oxidation state, compound **4** seemed to coordinate only to the ferrous heme but not to the ferric heme according to the spectral features in solution at room temperature. However, the crystal structure of nNOS−**4** revealed Fe−S thioether coordination at 2.7 Å.[8] Thus, there is a discrepancy with the nNOS−**4** complex: the spectroscopy suggests a noncoordinating high-spin complex in the ferric state, while the crystal structure shows strong continuous electron density between the sulfur and iron, indicative of iron coordination and a low-spin complex.

There are three possible explanations for this discrepancy: (1) heme iron reduction was triggered by X-ray exposure so that what is observed in the crystal structure is really a ferrous low-spin complex; (2) the heme active site in the crystal may experience structural restraints that do not exist in solution; or (3) since the crystallography is carried out at cryogenic temperatures (∼100 K) while the solution spectral work is at room temperature, there could be a temperature-dependent change in spin state. To monitor the changes of heme oxidation and spin state in crystals, we now have utilized *in situ* single-crystal spectrophotometry to follow the redox state of the iron during X-ray diffraction data collection. This enables a composite data collection strategy to be developed, which ensures that resulting electron density maps will be of mostly the ferric oxidized complex. In addition, we have used solution low-temperature EPR/ENDOR studies on nNOS complexed with three representative thioether inhibitors, **1**, **3**, and **4**, to further confirm the spin state and coordination environment. In another set of experiments, absorption spectra of nNOS in complex with the three inhibitors were also determined both in the crystal at room temperature and in solution (frozen glasses) at liquid nitrogen temperatures to monitor temperature effects.

METHODS

Protein Preparation and Crystallization. The heme domain of nNOS used in both structural and spectroscopic studies was prepared by limited trypsin digest of the partially purified full-length nNOS. The resulting heme-containing and FAD-containing fragments were further separated through a Superdex 200 gel filtration column (GE Healthcare) as described previously.[9] The buffer for the column was 50 mM Tris/HCl, pH 7.8, 10% glycerol, 5 mM βME, 10 μM H_4B, and 200 mM NaCl. No substrate L-arginine was added in order to make the heme active site available for inhibitor binding. The nNOS heme domain crystals were grown at 4 °C with the sitting drop vapor diffusion method as reported.[9] Protein at 7−9 mg/mL was premixed with 20 mM histidine before setting up 3−4 μL drops on coverglass over a 1 mL of well solution consisting of 22−24% PEG3350, 100 mM MES, pH 5.8, 140 mM ammonium acetate, 5 mM glutathione, and 35 μM SDS. Additional 10% (v/v) ethylene glycol was often needed to obtain better quality crystals. Crystals reached full size (about 0.08 × 0.08 × 0.03 mm^3) in 2 days and must be used within a week to ensure good diffraction quality. The thioether inhibitor soaks (10 mM) were carried out at 4 °C for 4−6 h after crystals had been passed in six increments through the cryo-protectant solution containing final concentrations of 25% PEG3350, 100 mM MES, pH 5.8, 100 mM ammonium acetate, 10% (v/v) glycerol, 10% (w/v) trehalose, 5% (w/v) sucrose, and 5% (w/v) mannitol. Crystals were flash cooled and stored in liquid nitrogen until data collection.

Single-Crystal Microspectroscopy at Synchrotron Beamlines. Single-crystal UV−visible absorption spectra were measured at beamlines 9-1 and 9-2 at SSRL. The spectroscopic system consists of 4DX microspectrophotometer (www.4dx.se) optics and 50 and 400 μm Xtreme solarization-resistant fiber cables, which guided the light delivered from a deuterium/halogen light source (model DH-2000-BAL; Ocean Optics Inc., www.oceanoptics.com; with output from 215 to 2000 nm) through the protein sample; the UV−visible spectra were recorded on a scientific grade spectrometer (model QE65000; Ocean Optics Inc.) under PC computer control with SpectraSuite (Ocean Optics, Inc.) software. Analysis plots and graphs were created with Microsoft Excel.

Rotation of the crystal sample, kept frozen to 100−110 K by Oxford Cryosystems, with the φ-axis of the beamline goniometer achieved favorable orientation for observing "solution-like" features. All measurements for each crystal were done in the same orientation. The physical orientation of the light path perpendicular to a crystal plane, going through the loop but not hitting the loop fiber, was often the most useful for collecting spectra. The spectroscopy system with 20 μm focus size on the sample was aligned to the 200 μm X-ray beam using the beamline sample video for both, assuring that relevant changes were measured.

After the best spectroscopic orientation was established, a baseline spectrum without X-rays was collected. Subsequent spectra were collected as a function of X-ray dose to determine the rate of photoreduction.

Composite Data Collection, Processing, and Structure Refinement. All X-ray data were obtained at 100 K. The X-ray triggered heme reduction for the nNOS−**4** complex crystal was monitored by the Q-band splitting in the visible region. The ferric heme absorption spectral features were found to survive for 3 min (less than 30% reduction) under X-ray exposure at wavelength 0.800 Å (0.15 × 0.15 mm^2 beam size) at SSRL beamline 9-1. The same beamline settings then were used for the composite data collections. For each crystal, a 10 s snapshot was taken for the purpose of indexing using MOSFLM,[10] then five frames of data with 1° oscillation and 30 s exposure per frame were collected. The total 160 s X-ray exposure, or 0.0227 mGy absorbed dose as calculated by RADDOSE,[11] for each crystal should represent less than 30% heme reduction. To minimize the number of crystals required for a complete data set, the strategy option in MOSFLM was used to determine where to collect the next 5° of data, based on the previously collected data.

The heme reduction in the nNOS−**3** crystal was monitored at SSRL beamline 9-2. The ferric heme was fully reduced in 60 s. The composite data collection of the nNOS−**3** complex was carried out at SSRL beamline 7-1 with an X-ray wavelength of 1.000 Å (beamline X-ray flux was about half that of beamline 9-2). For each crystal, a 5 s snapshot was used for indexing and strategy calculations. The five frames were collected from each crystal using a 1° oscillation and a 10 s exposure time. The 55 s X-ray exposure for each crystal was estimated to cause 50% heme reduction. Crystals received approximately 3 fold higher absorbed dose compared with nNOS−**4**: 0.0623 mGy as calculated by RADDOSE.

Data from each crystal were integrated separately using HKL2000,[12] and the resulting intensities were scaled together using SCALEPACK. Data frames that produced high R_{sym} (>15%) during scaling were rejected from the final composite data set. Some frames were also excluded based on the quality of the resulting electron density maps. A composite data set for nNOS−**4** with better than 90% completeness was obtained with 95° of data from 19 crystals, and for the nNOS−**3** data set, 65° of data from 13 crystals with better than 90% completeness were obtained. Additional improvements in the electron density maps were made by adjusting the resolution cutoff.

The scaled reflections were converted to MTZ format in CCP4 suite.[13] The structure refinements were carried out with REFMAC.[14] Structure visualization and model building were performed in COOT.[15] Once the inhibitor was modeled in, refined water molecules were added automatically with COOT using REFMAC. The TLS protocol[16] with each subunit as a TLS group was included in the final stage of refinement. Validation tools in COOT were used in the evaluation of the refined protein and water structures. The X-ray data collection and structure refinement statistics are summarized in Table 1. Coordinates of the nNOS−**3** and nNOS−**4** complexes refined against the composite data were deposited in the RCSB protein data bank with the entry codes of 3Q99 and 3Q9A, respectively.

EPR and ENDOR Measurements. The same nNOS sample used for the crystal structure and spectral studies was also used for the EPR measurements. The sample for ENDOR was exchanged into HEPES buffer (50 mM, pD 7.8, 5 mM GSH, 10 μM H_4B, 0.2 M NaCl) made in D_2O through extensive ultrafiltration using a Centricon (Millipore) device. The thiother inhibitors (10 μL of 20 mM) were added to the protein solution (70 μL of 300 μM) to make a final concentration of 260 μM.

The CW EPR/ENDOR measurements at 35 GHz were performed using a spectrometer described previously[17,18] using 100 kHz field modulation and dispersion mode detection under rapid passage conditions.[19] ENDOR spectra employed broadening of the RF to 100 kHz to improve signal-to-noise ratio.[20] For a single molecular orientation and for nuclei with a nuclear spin of $I = {}^1/_2$ (^{1}H), the ENDOR transitions for the $m_s = \pm{}^1/_2$ electron manifolds are observed at frequencies given by eq 1

$$\nu_{\pm} = |\nu_N \pm A/2| \quad (1)$$

where ν_N is the nuclear Larmor frequency and A is the orientation-dependent hyperfine coupling.

Single-Crystal Absorption Spectrophotometry at Room Temperature. Single-crystal absorption spectra were also taken at room temperature using an in-house system. The UV−visible S2000 miniature fiber optic spectrometer (Ocean Optics, Inc., Dunedin, Florida) is equipped with an AIS (Flemington, NJ) DL1000 light source (a tungsten−halogen bulb provides a visible light ranging from 400 to 900 nm). The spectrometer is controlled by OOIBase 32 software provided by the manufacturer. The crystal mounting stage was home-made. Two focusing lenses and two fiber optic cables (core dimension 100 μm) were used for the light path. Light from the light source was passed through one illumination optic fiber to the first lens and focused on the crystal, which was mounted on a goniometer head with a spindle stage (Supper). The scattered light after the crystal was refocused through the second lens into the read optic fiber leading to the spectrometer. Because the dimension of the incident light beam (~0.3 mm) was much larger than the crystal size (~0.1 mm) a piece of black paper with a 0.15 mm pinhole was also placed right behind the crystal to cut the beam size leading to the second focusing lens and spectrometer. With the pinhole in place, the integration time was adjusted to 60−70 ms, and 500 images were accumulated in order to record a reasonable spectrum. Crystals were oriented to produce the optimal signal, and reference and dark spectra were recorded.

Plate-like nNOS heme domain crystals (0.08 × 0.08 × 0.03 mm^3) were transferred to a nine-well depression plate (Hampton) containing 100 μL of an artificial mother liquor (25% PEG3350, 100 mM MES, pH 6.0, 100 mM ammonium acetate). Thioether inhibitors at 20 mM were added to the mother liquor to soak crystals for 3−4 h at 4 °C. The soaked crystals were then picked up with the nylon loop on a 18 mm mounting pin (Hampton) and dipped into immersion oil (type NVH, Hampton). Excess oil on the loop was removed by touching the loop to the surface of the depression plate until only a thin layer remained.

Absorption spectra of nNOS−inhibitor complex crystals in the oxidized (ferric) form were measured with the crystals treated as mentioned above, but reduction of crystals with excess of dithionite (dropping grains of dithionite into the solution) under aerobic conditions failed to give spectra of the reduced state. The reduction of crystals had to be achieved in a vinyl glovebox (COY Laboratory Instrument, Inc.). Crystals in the inhibitor (20 mM) containing mother liquor were degassed by evacuation and purged with argon alternately. Crystals brought into the glovebox were treated with ~50 mM dithionite. Soaking was continued for 3−4 h at room temperature. Crystals were then mounted in nylon loops and coated with immersion oil, as described above. Finally, each mounted crystal was placed in a labeled vial and sealed in a Ziploc bag inside the glovebox. Crystals were taken out of the Ziploc bag immediately before the spectral measurement.

Table 1. Composite Data Collection and Refinement Statistics

data set	nNOS−**3**	nNOS−**4**
PDB code	3Q99	3Q9A
	Data Collection	
space group	$P2_12_12_1$	$P2_12_12_1$
cell dimensions *a*, *b*, *c* (Å)	52.16, 111.42, 164.21	51.82, 110.65, 164.23
resolution (Å)	2.15 (2.19−2.15)	2.25 (2.29−2.25)
R_{sym}	0.084 (0.41)	0.101 (0.65)
$I/\sigma I$	12.1 (1.7)	12.7 (1.8)
no. unique reflns	48 312	43 855
completeness (%)	91.1 (91.3)	95.5 (93.9)
redundancy	2.5 (2.5)	3.4 (3.2)
no. of crystals	13	19
	Refinement	
resolution (Å)	2.15	2.25
no. reflns	45 856	41 571
R_{work}/R_{free} [a]	0.190/0.239	0.186/0.236
no. atoms		
protein	6664	6680
ligands/ions	159	159
water	265	219
Wilson *B*-factor (Å^2)	34.4	37.4
mean *B*-factor (Å^2)	36.8	41.2
rms deviations		
bond lengths (Å)	0.013	0.012
bond angles (deg)	1.398	1.500

[a] R_{free} was calculated with the 5% of reflections set aside randomly throughout the refinement.

Solution (Frozen Glasses) Absorption Spectrometry at Low Temperature. The purified nNOS heme domain protein stored at −80 °C in Tris buffer[9] was thawed and further concentrated to ~80 mg/mL in the presence of 0.5 M NaCl and 30% glycerol. To 10 μL of this protein solution, 10 mM of each of compound **1**, **3**, and **4** was added, and the incubation was continued at 4 °C for 4 h. The nNOS−thioether complex solutions in the ferric state (at ~1.2−1.4 mM high concentration) were scooped up with the nylon loops (0.2 mm thickness) and frozen in liquid nitrogen.

The remaining nNOS−thioether solutions (4 μL of each type) were then placed in a nine-well depression plate (Hampton) and brought into a glovebox. To each protein droplet was added 2−3 grains of dithionite under a microscope. Solutions were incubated for 20−30 min. The reduced nNOS−thioether solutions were then scooped with nylon loops, placed in cryo-vials, and individually sealed in the Ziploc bags before being brought out of the glovebox for freezing.

Table 2. UV−Visible Absorption Spectral Features of nNOS−Thioether Complexes

sample	condition	temperature[a]	redox state	Soret [shoulder] (nm)	Q-band (nm)	charge transfer (nm)	spin state
nNOS−**1**	solution	RT	Ferric	395	broad	647	HS
	frozen glasses	LN_2	Ferric	395	491	645	HS
	solution	RT	Ferrous	411	552	--	HS
	frozen glasses	LN_2	Ferrous	411	550	--	HS
nNOS−**3**	solution	RT	Ferric	423	547	--	LS
	frozen glasses	LN_2	Ferric	421	542	--	LS
	crystal	RT	Ferric	--	548	--	LS
	crystal	LN_2	Ferric	--	547	646	LS
	solution	RT	Ferrous	444	544, 566	--	LS
	frozen glasses	LN_2	Ferrous	440	540, 564	--	LS
	crystal	RT	Ferrous	--	541, 568	--	LS
	crystal	LN_2	Ferrous	--	540, 564	--	LS/HS
nNOS−**4**	solution	RT	Ferric	399	broad	649	HS
	frozen glasses	LN_2	Ferric	418	542	645	LS
	crystal	RT	Ferric	--	broad	648	HS
	crystal	LN_2	Ferric	--	540	648	LS
	solution	RT	Ferrous	413 [440]	555	--	HS/LS
	frozen glasses	LN_2	Ferrous	436	537, 562	--	LS/HS
	crystal	RT	Ferrous	--	561	--	HS
	crystal	LN_2	Ferrous	--	536, 563	--	LS

[a] RT, room temperature (298 K); LN_2, liquid nitrogen gas cryostat temperature (~100 K).

The UV−visible absorption spectral measurements of protein solutions were carried out at SSRL on BL9-1 with the same instrument setup that was used for the single-crystal spectral work described earlier. Most of the solution spectra were collected with the liquid nitrogen cooling at ~110 K. Protein solutions with 30% glycerol remained clear at temperatures below 200 K. Temperature-dependent studies were performed with an Oxford Cryosystem cryostat under Blu-Ice/DCS beamline control. Spectral measurements were made after each 20−40 K increment in temperature, waiting ~1 min for the temperature to stabilize.

RESULTS AND DISCUSSION

Heme in Crystal Is Reduced by X-ray Exposure. In the presence of compound **4**, nNOS exhibits a spectrum typical of a high-spin species with a Soret peak at 399 nm in solution at room temperature (Table 2). Upon heme reduction, the spin state undergoes a partial transition from high spin to low spin, indicated by a shoulder on the Soret peak at 440 nm.[8] However, the 2.25 Å crystal structure of nNOS−**4** at 100 K reveals a Fe−S thioether distance of 2.7−2.8 Å with continuous electron density between the iron and sulfur suggesting a low-spin complex. The discrepancies between the high-spin spectral features in solution at room temperature and the low-spin-like crystallographic data at 100−110 K were initially interpreted as the result of heme iron reduction in the crystal during X-ray data collection. This suspicion was supported by the observation that the 2.1 Å resolution structure obtained at 100 K from the nNOS−**4** crystal (PDB code 3JT9) prereduced with dithionite was the same as the structure obtained from the nNOS−**4** crystal that started in the ferric oxidized state.[8]

The spectral changes monitored at various X-ray exposure times for nNOS−**3** and nNOS−**4** are shown in Figure 1. For compound **3**, the single visible peak at 547 nm represents the ferric, low-spin state.[8] This single peak splits into two peaks upon heme reduction, 540 and 564 nm, which was also observed in solution at room temperature (Table 2). With the Q-band splitting as an indicator of heme reduction, the ferric heme of nNOS is fully reduced within about 1 min in the presence of compound **3** at SSRL beamline 9-2 (Figure 1A). At beamline 9-1, with a much weaker X-ray source, reduction of the ferric heme of nNOS−**4** starts in about 3 min, judging by the Q-band splitting at 536 and 563 nm from the single peak at 540 nm, although it takes more than 20 min to reach full reduction (Figure 1B). This single Q-band at 540 nm and the 650 nm charge transfer band before X-ray exposure presumably represents the starting ferric state. However, the spin state in the crystal is uncertain at this point because the Q-band is shown as a broad peak for a high-spin, ferric nNOS−**4** in the absolute spectrum in solution.[8] The Q-band splitting and disappearance of the 650 nm band correspond to the coordination of compound **4** to the ferrous heme. For nNOS−**4** in solution at room temperature the 650 nm peak vanished upon heme reduction, although the Q-band splitting was not apparent because only a small fraction of nNOS had the low-spin feature judging from the intensity of the 440 nm shoulder of the Soret peak at 413 nm, the latter represented the high-spin, ferrous heme (Table 2).[8]

Single-crystal spectral measurements were also performed with the nNOS−**3** crystal prereduced by dithionite. Figure 2 shows that the 650 nm charge transfer band does not appear in the ferrous state. In addition, the Q-band splitting is present at the beginning of data collection and remains relatively unchanged during the entire course of experiment. This further confirms the Q-band splitting can be used as the indicator of binding of inhibitor to the ferrous heme.

Composite NOS Structures in the Ferric State. Data from a total of 13 nNOS−**3** crystals that were exposed to X-rays for only 60 s and 0.0623 mGy absorbed dose each were merged to give a complete composite data set to ~2.15 Å resolution. The nNOS−**3** structure refined against the composite data represents a mixed oxidation state of ~50% ferric and ~50% ferrous. The

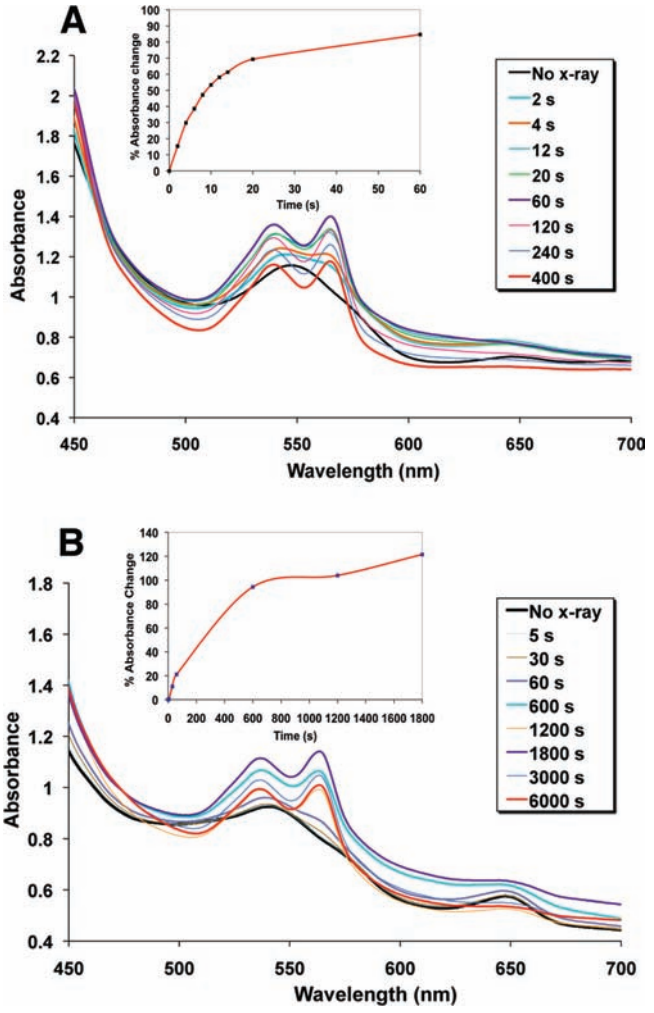

Figure 1. Single-crystal absorption spectra recorded at 100 K during X-ray data collection for (A) nNOS−**3** at SSRL BL9-2 and (B) nNOS−**4** at BL9-1. The largest dimension of crystals was about 80 μm while the spectrometer had a beam focus size at 20 μm. Shown in the insets is the % change in the absorbance difference ($\Delta A = A_{564nm} - A_{648nm}$) versus the X-ray exposure time as an indication of the heme reduction.

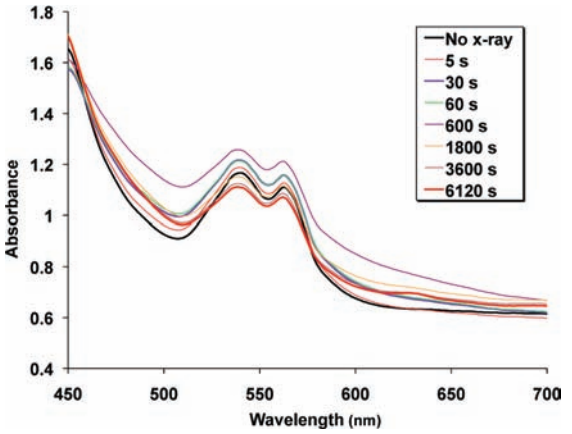

Figure 2. Single-crystal absorption spectra recorded at SSRL BL9-1 for a dithionite reduced nNOS−**3** crystal at 100 K during X-ray data collection. Experimental conditions are similar to those in Figure 1.

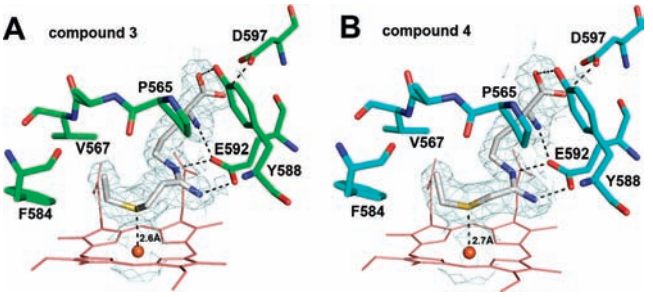

Figure 3. The active site in nNOS−**3** (A) and nNOS−**4** (B) derived from low-dose composite data sets. Around each thioether inhibitor is the sigmaA weighted $2F_o - F_c$ electron density contoured at 1 σ. Major hydrogen bonds between enzyme and inhibitor are shown as dashed lines. The Fe−S thioether distance is labeled. The atomic color schemes are N, blue; O, red; S, yellow. The figure was prepared with PyMol (http://www.pymol.org).

Fe−S thioether bond length in the resulting structure (Figure 3A) is 2.6 Å, which is not significantly different from the bond length for the predominantly ferrous nNOS−**3** structure determined using a normal X-ray dose.[8] The composite data set obtained for the nNOS−**4** structure (Figure 3B) was assembled from 19 crystals, receiving 0.0223 mGy absorbed dose each, to 2.25 Å resolution and represents predominantly the ferric state. The Fe−S thioether bond length of 2.7 Å in this structure is also similar to the bond length in the predominantly ferrous structure.[8]

Thus the structures of nNOS bound with compound **3** in the ferric/ferrous mixed states or with compound **4** in the mostly ferric state did not show any significant difference in Fe−S thioether distance from those obtained from X-ray structures in the ferrous state. It is reasonable to assume that large changes in the Fe−S thioether bond length would not be observed for the ferric and ferrous states of nNOS−**3** since solution spectroscopy indicates a low-spin complex in both the ferric and ferrous forms. However, for nNOS−**4** to have a similar Fe−S thioether distance when the heme iron is reduced from ferric to ferrous was not expected since room-temperature spectroscopy indicates high spin in the ferric state and a mixed spin in the ferrous state. At the time, we had the conventional concept that in a high-spin state the distal Fe−S thioether bond should be broken as in the case with the nNOS−**1** structure (PDB code 3JT3).[8] The crystal structures at 2.1−2.2 Å, as in this study, have an overall coordinate error about 0.2 Å. The resolution should be good enough to distinguish whether a ligation bond exists. However, all the structural results indicate that changes in Fe−S thioether distance due to the spin state in nNOS−**4** are small and within the experimental error of 0.2 Å.

Spin State Determination by EPR/ENDOR Experiments. Figure 4a shows the 35 GHz CW EPR spectra at 2 K of nNOS as isolated and in the presence of inhibitors **1**, **3**, and **4**. Integration of the EPR spectrum of the ferric heme from as-isolated nNOS is a mixture of 64% low-spin and 36% high-spin components. The *g*-values for the high-spin ($g_1 = 7.66, g_2 = 4.07$) and low-spin ($g_1 = 2.45$, $g_2 = 2.30$, $g_3 = 1.90$) states are similar to those reported earlier.[21] In the high-spin state, the Fe(III) is penta-coordinated, whereas in the low-spin state it is hexa-coordinated, with water as the sixth ligand. With the addition of inhibitor **1** to nNOS, the spin-state equilibrium shifts to the high-spin form; the EPR

dx.doi.org/10.1021/ja201466v |*J. Am. Chem. Soc.* 2011, 133, 8326–8334

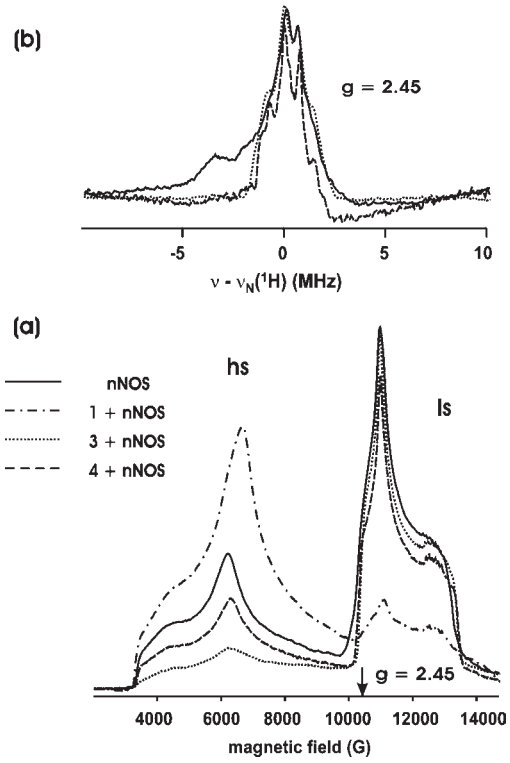

Figure 4. (a) CW EPR spectrum (35 GHz) of ferric nNOS showing the effect of inhibitor binding (**1**, **3**, **4**) to nNOS. Sample labels legend is added as an inset; hs represents the Fe(III) in a $S = {}^5/_2$ spin state, and ls represents the $S = {}^1/_2$ spin state. Conditions: T = 2 K, modulation amplitude, 1 G, MW frequency, 34.82 GHz. (b) CW ^{1}H ENDOR spectra (35 GHz) for nNOS alone and with inhibitor **3** or **4** bound measured at g = 2.45 (centered at the ^{1}H Larmor frequency). Conditions and labels are as in panel a.

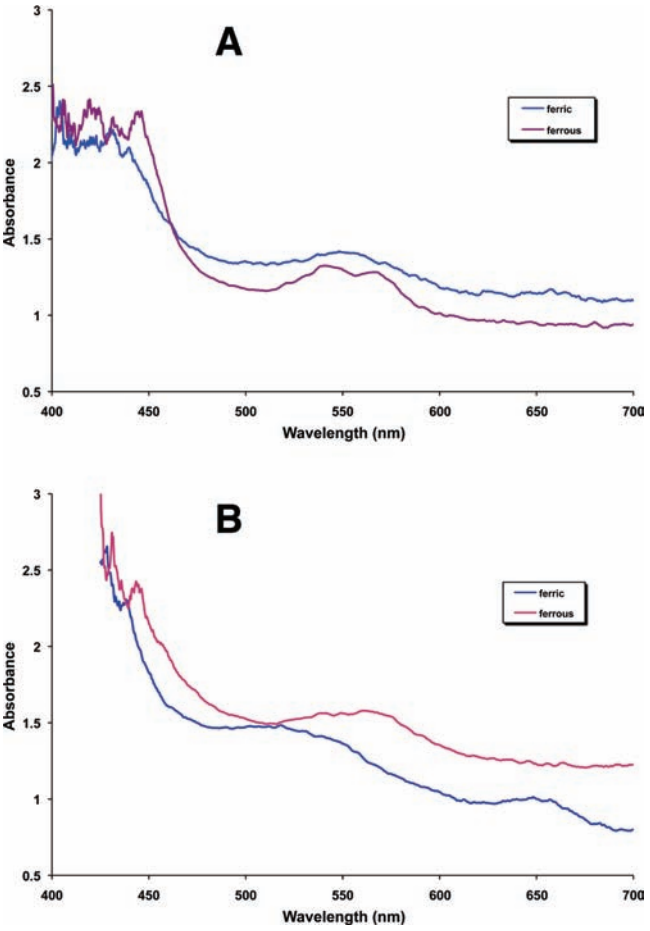

Figure 5. Room-temperature single-crystal absorption spectra of the nNOS heme domain with either compound **3** (A) or compound **4** (B) bound. The spectrum for each of the two heme oxidation states was taken with a different crystal.

spectrum shows predominantly the high-spin state with only a small, 15%, low-spin component, indicating that binding of **1** displaces water bound to Fe(III) without itself providing a ligand, leaving the Fe(III) as five-coordinated. In contrast, the addition of **3** shifts the spin-state equilibrium in favor of 85% low-spin, with a nearly 3-fold increase in the low-spin/high-spin state ratio compared with nNOS alone. When inhibitor **4** binds, the EPR spectrum again shows a mixture of Fe(III) in both high-spin (30%) and low-spin (70%) states.

To determine the ferriheme coordination state in the inhibitor complexes, ENDOR spectroscopy was carried out on as-isolated nNOS, **3** + nNOS, and **4** + nNOS. Figure 4b shows the ^{1}H ENDOR spectra for the three samples at g = 2.45 corresponding to g_1 of the low-spin ferriheme spectra. The ENDOR spectrum of the substrate-free, as-isolated nNOS shows an intense cluster of weakly coupled peaks centered at the ^{1}H Larmor frequency that are associated with the heme or nearby protein residues. In addition, it shows a ν feature from a $\nu+/\nu-$ pair (eq 1) from protons of the H_2O axial ligand[22] with maximum hyperfine coupling $A \approx 8$ MHz at g = 2.45; it is common for relaxation effects to cause one of the $\nu+/\nu-$ partners to be weak or absent. This proton signal from low-spin Fe(III) disappears when either **3** or **4** binds to nNOS, indicating that the water bound to Fe(III) is displaced. Because there must be a sixth ligand to produce the low-spin state, we infer that the H_2O is replaced by sulfur of the thioether in inhibitors **3** and **4**.

Single-Crystal Absorption Spectrophotometry at Room Temperature. Given the crystal structure and EPR data, there is little doubt that at low temperature both compounds **3** and **4** form the low-spin complex with nNOS regardless of the heme oxidation state. If the heme reduction itself cannot explain the discrepancy in the spin-state change of nNOS−**4** observed in the room-temperature solution spectra and the low-temperature experiments including crystal structure and EPR data, then the issue may be a temperature-dependent spin-state transition.

To this end, we first examined the room-temperature single-crystal absorption spectra with the cysteine-thiolate ligated nNOS heme domain crystals soaked with thioether compounds **3** and **4** in both the oxidized and dithionite-reduced states. Figure 5 shows that these two compounds exhibit the same spectral features at room temperature in the crystal and in solution (Table 2). For example, **3** forms a low-spin complex with ferric nNOS with a single visible band at 547 nm in solution[8] and a single peak at 548 nm in the crystal (Figure 5A). With the reduced heme iron, the visible Q-band splits into two peaks that are observed in both the solution and the single-crystal spectra. In the solution spectrum, we reported previously[8] that compound **4** showed typical high-spin features with a broad visible peak around 530 nm and a charge transfer peak at 650 nm in the ferric state. The same spectral profiles are seen from the

dx.doi.org/10.1021/ja201466v | J. Am. Chem. Soc. 2011, 133, 8326–8334

single-crystal spectra in the oxidized form (Figure.5B and Table 2). For the ferrous heme with compound **4**, both solution and single-crystal spectra show identical results: a not quite resolved Q-band near 560 nm and disappearance of the charge transfer band at 650 nm. These features are consistent with a high-spin, ferrous heme−thioether complex. Since the room-temperature solution and single-crystal spectra are the same, then the crystal lattice is not imposing some peculiar property to the active site that significantly differs from solution, at least with respect to inhibitor-induced spin shifts.

This should be contrasted with results in Figure 1. In the crystal at 100 K, the ferrous nNOS−**4** complex is low-spin, while the ferrous nNOS−**4** complex at room temperature remains high-spin, both in solution and in the crystal. Therefore, it appears that a decrease in temperature switches ferrous nNOS−**4** from high-spin to low-spin.

Solution (Frozen Glasses) Absorption Spectrophotometry at Low Temperature. So far, the low-spin state of the nNOS−**4** complex was only observed at low temperature in crystal structures, single-crystal spectra, and EPR spectra. The one final piece of information required was the solution spectrum at low temperature. To do this experiment, a concentrated solution of nNOS at 1.2−1.4 mM was scooped in the loop normally used for crystal mounting and frozen, and spectra were recorded using the same instrument employed for single-crystal spectroscopy. As we hypothesized, the spin state in the nNOS−**4** complex changes as the temperature is lowered. As shown in Figure 6, the nNOS low-temperature frozen solution spectra in the presence of compound **1**, **3**, and **4** are the same as in the low-temperature crystal spectra in both the ferric and ferrous heme oxidation states. nNOS−**4** exhibits (Figure 6C) low-spin spectral features both in the ferric (Soret peak at 418 nm and single Q-band at around 540 nm) and in the ferrous (Soret at 436 nm and split Q bands at 537 and 562 nm) states (Table 2). Therefore, at low temperature, nNOS−**4** shares the same low-spin spectral features as that of nNOS−**3** (Figure 6B). This explains why the two complex structures, nNOS−**3** and nNOS−**4**, determined at low temperature, showed similar Fe−S thioether interactions. By comparison of the spectral features, it is now clear that the starting state of the nNOS−**4** crystal (Figure 1B) is predominantly ferric and low-spin, characteristic with a single Q-band at 540 nm, although a more pronounced charge transfer band at 650 nm is observed in the crystal spectrum than is seen in the frozen glasses. On the other hand, compound **1** remains high-spin even at low temperature with a ferric Soret peak at 395 nm and a charge transfer band at 645 nm, while in the ferrous state with a Soret at 411 nm and a Q-band at 550 nm. These results are consistent with the high-spin EPR spectrum for this compound (Figure 4) and with the crystal structure of nNOS−**1** (3JT3) where there is no Fe−S thioether ligation bond.[8]

Learning that lowering the temperature changes the spin state, we further explored the spin-state transition as a function of temperature. The spectral changes of nNOS−**4** in both the ferric and ferrous states as a function of temperature are shown in Figure 7. With ferrous heme, nNOS−**4** exhibits a low-spin (Soret at 436 nm and split Q bands) to high-spin (Soret at 416 nm and a single Q-band at 557 nm) transition (Figure 7A) upon a temperature increase to 270 K. The transition occurred in a temperature range above 200 K. To our surprise, the spectral changes upon a temperature increase for nNOS−**4** were also observed in the ferric state (Figure 7B) that correspond to a low-spin (Soret at 418 nm and single Q-band) to high-spin (Soret at around 400 nm and broadening of the Q-band) transition. The temperature dependence of the spin-state transition for nNOS−**4** is reversible, which is clearly demonstrated when the samples are cooled back to 100 K, as shown in Figure 7. These results indicate that compound **4** is a low-spin heme ligand at low temperature regardless of the heme oxidation state

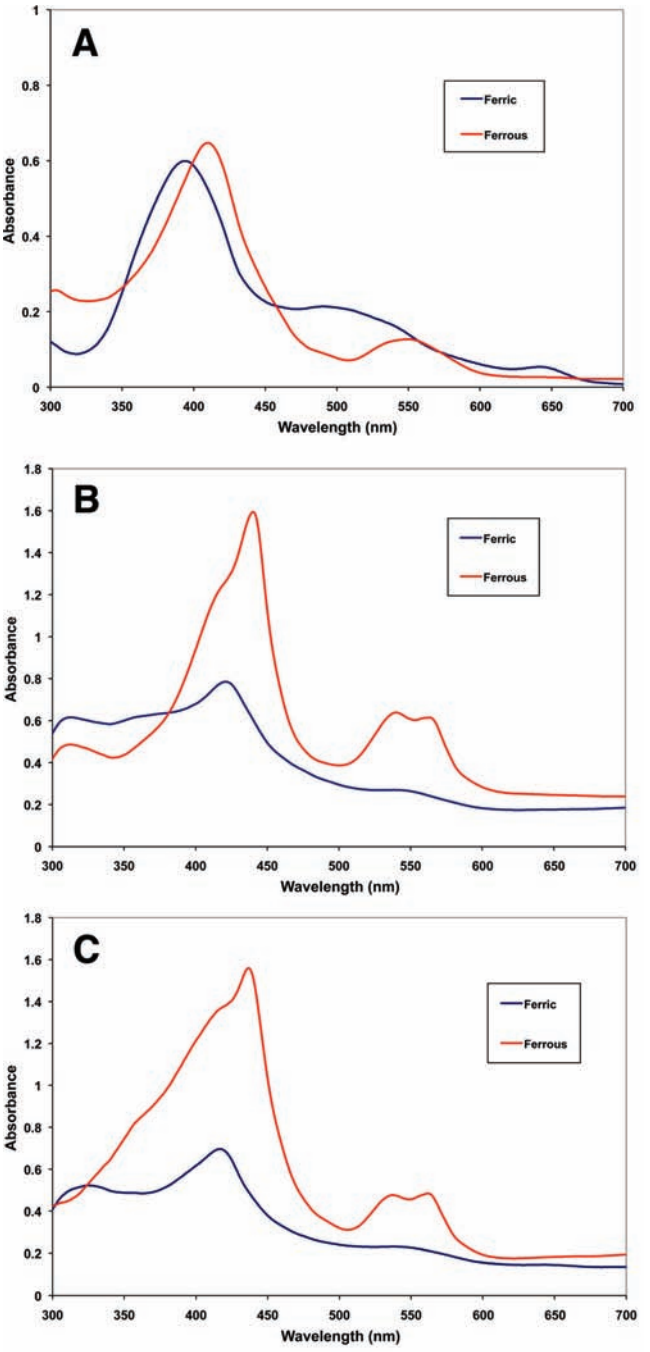

Figure 6. The solution (frozen glasses) absorption spectra of nNOS in complex with compound **1** (A), **3** (B), and **4** (C) at ∼110 K. Spectra of the ferric and ferrous states were taken for each nNOS−thioether inhibitor complex with different samples. Protein samples at high concentration of 1.2−1.4 mM in the presence of 0.5 M NaCl and 30% glycerol were scooped with 0.2 mm nylon loop and then flash-cooled in liquid nitrogen.

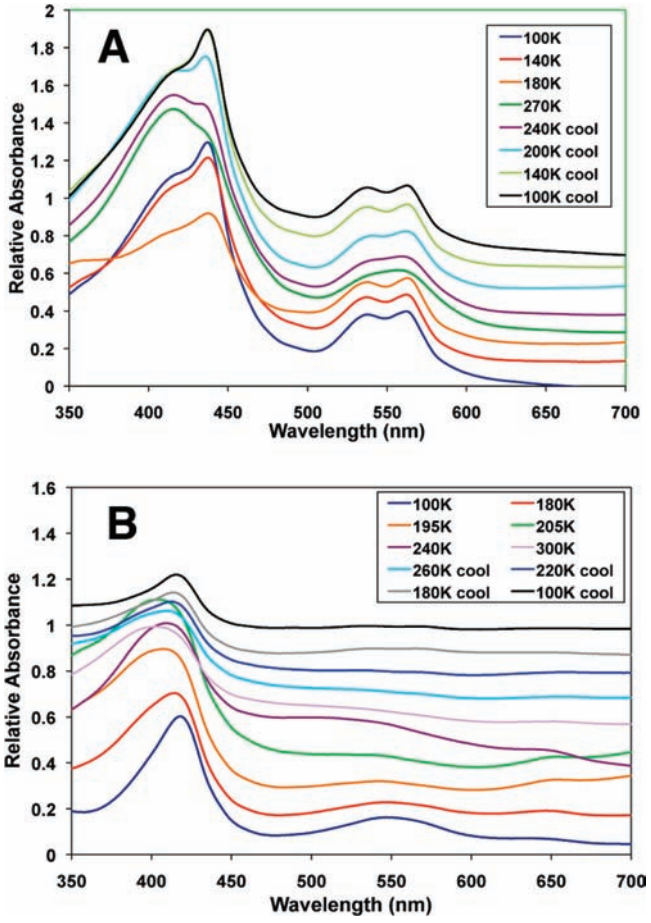

Figure 7. The temperature-dependent spin-state transitions observed for nNOS in complex with compound **4** in either the ferrous state (A) or the ferric state (B) frozen glasses. To clearly illustrate the spectral changes at each temperature, all the spectra have been normalized at 600 nm and then offset by 0.1 absorbance unit from each other.

but is a high-spin ligand above 200 K. In contrast, compound **3** behaves as a low-spin heme ligand for both heme oxidation states without the temperature dependence as for compound **4**.

Spin Crossover. The temperature-dependent spin-state transition that we observed for nNOS−**4** complex is consistent with the so-called "spin crossover" phenomenon reported for many transition metal−ligand complexes[23,24] and is best explained by ligand field theory.[25] The key concept is the balance between the spin-pairing energy (electron−electron repulsion) and the ligand field strength expressed by a parameter 10Dq, which measures the gap between two metal d orbital energy levels, for instance, the e_g and t_{2g} levels in octahedral coordination geometry. When 10Dq is larger than the pairing energy, d electrons tend to pair up in the low-energy orbitals giving a low-spin state; if 10Dq is small with a weak field ligand compared with pairing energy, then d electrons will unpair into d orbitals in both energy levels leading to a high-spin state. The field strength parameter, 10Dq, is a function of the metal−ligand distance (r) as $1/r^n$ (n = 5−6).[25,26] Therefore, contraction of the metal−ligand distance (on the order of 0.1−0.2 Å[27]) at low temperature will increase the field strength to the extent that tips the balance between 10Dq and spin-pairing energy, causing the spin crossover toward the low-spin state. The spin crossover phenomenon is not caused by the formation or breaking of a ligation bond, which is different from the commonly observed spin state shifts in heme proteins that often result from the changes in heme coordination. For instance, addition of imidazole to the L-arginine-bound nNOS will change its pentacoordinated, high-spin Soret peak at 395 nm to a typical low-spin Soret peak at 427 nm because of its newly formed Fe−N ligation bond.

The thioether nNOS inhibitors in this study are S-donating heme ligands with modest field strength, similar to the S-containing ligand, dithiocarbamate, first discovered to cause the spin crossover in Fe(III) complexes.[28] The rather weak ligation strength of these thioethers has been demonstrated by the lack of heme coordination in the absence of proper hydrophobic interactions with the protein in the cases of compounds **1** and **2**. The strongest field strength among the series is shown by compound **3** and is due to the optimal interactions from its ethyl tail to the hydrophobic pocket defined by Phe584 and Val567. In comparison, compound **4** has a slightly weaker field strength than **3**. At room temperature, it only exists in a high-spin state, both in solution and in the crystal, even though the thioether S atom is very likely within a weak ligation distance from the heme iron, presumably in the range of 2.8−2.9 Å. Upon lowering of the temperature below ∼200 K, the contraction of the Fe−S thioether distance causes an increase in the ligand field strength forcing the pairing of iron d electrons into the lower energy orbitals, leading to low spin. This spin crossover for nNOS−**4** occurs in both the ferric and ferrous states as shown in our temperature-dependent solution (frozen glasses) spectral data (Figure 7). By careful inspection of the low-temperature solution spectra, we have noticed that even for nNOS−**3** in the ferrous state the Soret peak has a small shoulder on the high-energy side. This shoulder may represent a small population of complex that is still in the high-spin state (see the spectral features shown by the high-spin compound **1** in Figure 6A). For nNOS−**4**, this shoulder is even more pronounced, indicating that an even higher population of high-spin complex existed. A distribution of high- and low-spin states in nNOS−**3** and nNOS−**4** is also apparent in the EPR data in the ferric state (Figure 4). The spin state distribution should be dependent on the relative field strength of each thioether inhibitor, while the ligand field strength is, in turn, controlled by how optimal the hydrophobic interactions are between the alkyl tail of each inhibitor and protein, as demonstrated in our nNOS−thioether complex structures.[8]

One last piece of information missing from this study is the Fe−S thioether distance in nNOS−thioether complex in crystals at room temperature. Unfortunately, obtaining room-temperature ferric structures at the resolution required is not feasible given the instability of nNOS crystals at room temperature. As a result, it is not possible to determine whether the S−Fe bond breaks at room temperature to give a true pentacoordinate complex where the S−Fe distance is in the 3−4 Å range, although such a large change appears unlikely given the constraints of the inhibitors in the active site. It is more likely that the switch in spin-state is due to a small 0.1−0.2 Å increase in the Fe−S distance that is associated with the low- to high-spin transition.

■ CONCLUSIONS

In summary, we have found that in the absence of very high resolution, it is difficult to assign a spin state to heme−ligand complexes based on the Fe−S thioether bond length in the crystal structure, particularly with inherently weak thioether

complexes where a Fe−S thioether bond breaking may not be involved in the low- to high-spin transition. However, the apparent inconsistency between cryogenic crystal structures, single-crystal spectroscopy, and room-temperature UV−visible spectroscopy now has been resolved by employing several approaches. The combination of EPR/ENDOR, single-crystal and solution UV−visible spectroscopy as a function of temperature, and careful composite X-ray data collection protocols has resolved these inconsistencies resulting in a picture readily understood using basic ligand field concepts. The spin crossover we observed has been rarely reported in proteins but is potentially important, considering current interests in utilizing spin crossover complexes in material sciences.[29] Finally, this effort underscores the exquisite sensitivity of spectral methods to very subtle changes in heme−ligand parameters that are often undetectable in moderate resolution protein crystal structures.

AUTHOR INFORMATION

Corresponding Author
poulos@uci.edu

ACKNOWLEDGMENT

Portions of this research were carried out at the Stanford Synchrotron Radiation Lightsource, a Directorate of SLAC National Accelerator Laboratory and an Office of Science User Facility operated for the U.S. Department of Energy Office of Science by Stanford University. The SSRL Structural Molecular Biology Program is supported by the DOE Office of Biological and Environmental Research, and by the National Institutes of Health, National Center for Research Resources, Biomedical Technology Program (Grant P41RR001209), and the National Institute of General Medical Sciences. The authors are grateful for financial support from the National Institutes of Health (Grant GM057353 to T.L.P. and Grant GM049725 to R.B.S.). H.L. thanks Prof. J. K. Lanyi for his instructions in running the single-crystal spectrophotometer and also acknowledges the excellent technical assistance from Dr. Yergalem Meharenna and Hoda Abou-Ziab.

REFERENCES

(1) Knowles, R. G.; Moncada, S. *Biochem. J.* **1994**, *298*, 249–258.
(2) Griffith, O. W.; Stuehr, D. J. *Annu. Rev. Physiol.* **1995**, *57*, 707–736.
(3) Moncada, S.; Palmer, R. M.; Higgs, E. A. *Pharmacol Rev.* **1991**, *43*, 109–142.
(4) Kerwin, J. F., Jr.; Lancaster, J. R., Jr.; Feldman, P. L. *J. Med. Chem.* **1995**, *38*, 4343–4362.
(5) Babu, B. R.; Griffith, O. W. *Curr. Opin. Chem. Biol.* **1998**, *2*, 491–500.
(6) Hobbs, A. J.; Higgs, A.; Moncada, S. *Annu. Rev. Pharmacol. Toxicol.* **1999**, *39*, 191–220.
(7) Litzinger, E. A.; Martasek, P.; Roman, L. J.; Silverman, R. B. *Bioorg. Med. Chem.* **2006**, *14*, 3185–3198.
(8) Martell, J. D.; Li, H.; Doukov, T.; Martasek, P.; Roman, L. J.; Soltis, M.; Poulos, T. L.; Silverman, R. B. *J. Am. Chem. Soc.* **2010**, *132*, 798–806.
(9) Li, H.; Shimizu, H.; Flinspach, M.; Jamal, J.; Yang, W.; Xian, M.; Cai, T.; Wen, E. Z.; Jia, Q.; Wang, P. G.; Poulos, T. L. *Biochemistry* **2002**, *41*, 13868–13875.
(10) Leslie, A. G. W. *Jnt. CCP4/ESF-EACMB Newslett. Protein Crystallogr.* **1992**, 26.
(11) Murray, J. W.; Garman, E. F.; Ravelli, R. B. G. *J. Appl. Crystallogr.* **2004**, *37*, 513–522.
(12) Otwinowski, Z.; Minor, W. *Methods Enzymol.* **1997**, *276*, 307–326.
(13) Number4, C. C. P. *Acta Crystallogr.* **1994**, *D50*, 760–763.
(14) Murshudov, G. N.; Vagin, A. A.; Dodson, E. J. *Acta Crystallogr.* **1997**, *D53*, 240–255.
(15) Emsley, P.; Cowtan, K. *Acta Crystallogr.* **2004**, *D60*, 2126–2132.
(16) Winn, M. D.; Isupov, M. N.; Murshudov, G. N. *Acta Crystallogr.* **2001**, *D57*, 122–133.
(17) Davoust, C. E.; Doan, P. E.; Hoffman, B. M. *J. Magn. Reson.* **1996**, *119*, 38–44.
(18) Werst, M. M.; Davoust, C. E.; Hoffman, B. M. *J. Am. Chem. Soc.* **1991**, *113*, 1533–1538.
(19) Mailer, C.; Hoffman, B. M. *J. Phys. Chem.* **1976**, *80*, 842–846.
(20) Hoffman, B. M.; Derose, V. J.; Ong, J. L.; Davoust, C. E. *J. Magn. Reson.* **1994**, *110*, 52–57.
(21) Salerno, J. C.; Frey, C.; McMillan, K.; Williams, R. F.; Masters, B. S.; Griffith, O. W. *J. Biol. Chem.* **1995**, *270*, 27423–27428.
(22) Davydov, R.; Sudhamsu, J.; Lees, N. S.; Crane, B. R.; Hoffman, B. M. *J. Am. Chem. Soc.* **2009**, *131*, 14493–14507.
(23) Gutlich, P.; Goodwin, H. A. In *Topics in Current Chemistry*; Gutlich, P., Goodwin, H. A., Eds.; Springer-Verlag: Berlin, 2004; Vol. 233, pp 1−47.
(24) van Koningsbruggen, P. J.; Maeda, Y.; Oshio, H. In *Topics in Current Chemistry*; Gutlich, P., Goodwin, H. A., Eds.; Springer-Verlag: Berlin, 2004; Vol. 233, pp 259−324.
(25) Hauser, A. In *Topics in Current Chemistry*; Gutlich, P., Goodwin, H. A., Eds.; Springer-Verlag: Berlin, 2004; Vol. 233, pp 49−58.
(26) Schlafer, H. L.; Gliemann, G. *Einfuhrung in die ligandenfeldtheoris*; Akad Verlagsgesellschaft: Wiesbaden, 1980.
(27) Guionneau, P.; Marchivie, M.; Bravic, G.; Letard, J.-F.; Chasseau, D. In *Topics in Current Chemistry*; Gutlich, P., Goodwin, H. A., Eds.; Springer-Verlag: Berlin, 2004; Vol. 234, pp 97−128.
(28) Cambi, L.; Szego, L. *Ber. Dtsch. Chem. Ges.* **1931**, *64*, 167.
(29) Letard, J.-F.; Guionneau, P.; Goux-Capes, L. In *Topics in Current Chemistry*; Gutlich, P., Goodwin, H. A., Eds.; Springer-Verlag: Berlin, 2004; Vol. 235, pp 221−249.